Chemometrics and Intelligent Laboratory Systems 107 (2011) 165–173

Contents lists available at ScienceDirect

Chemometrics and Intelligent Laboratory Systems

journal homepage: www.elsevier.com/locate/chemolab

A Bayesian inversion method for estimating the particle size distribution of latexes from multiangle dynamic light scattering measurements

Luis A. Clementi [a,b], Jorge R. Vega [a,b,*], Luis M. Gugliotta [a], Helcio R.B. Orlande [c]

[a] INTEC (CONICET and Universidad Nacional del Litoral), Güemes 3450 (3000), Santa Fe, Argentina
[b] FRSF-UTN (Facultad Regional Santa Fe, Universidad Tecnológica Nacional), Lavaisse 610 (3000), Santa Fe, Argentina
[c] DEM/PEM-Politécnica/COPPE (Federal University of Rio de Janeiro, UFRJ), Cidade Universitária (68503), 21941-972, Rio de Janeiro, Brazil

ARTICLE INFO

Article history:
Received 3 January 2011
Received in revised form 2 March 2011
Accepted 6 March 2011
Available online 12 March 2011

Keywords:
Latex
Particle size distribution
Dynamic light scattering
Inverse problem
Regularization techniques
Bayesian method

ABSTRACT

A statistical Bayesian method is proposed for estimating the particle size distribution (PSD) of polymeric latexes from multiangle dynamic light scattering (MDLS) measurements. The procedure includes two main steps: 1) the calculation of the angle-dependent average diameters of the PSD from the MDLS autocorrelation measurements, and 2) the PSD estimation through a Bayesian method (that is solved with a Markov chain Monte Carlo sampling strategy implemented in the form of a Metropolis–Hasting algorithm). First, the method was evaluated through two simulated examples that involved unimodal and bimodal PSDs of different shapes. Then, the method was employed for estimating two bimodal PSDs obtained by mixing two narrow polystyrene standards. For comparison, all examples were also solved by numerical inversion of the raw MDLS autocorrelation measurements through a classical regularization technique typically used for inverting ill-conditioned linear problems. The proposed method appears as an effective and robust tool for characterizing unimodal or multimodal PSDs without requiring any a priori assumption on the number of modes or on their shapes. For unimodal PSDs exhibiting high asymmetries and for bimodal PSDs with modes of different particle concentration, the Bayesian method produced more accurate results than those obtained with the classical regularization technique.

1. Introduction

A polymer colloid (or latex) is normally constituted by sub-micrometric polymer particles dispersed in an aqueous medium. In industry, synthetic latexes are typically obtained through aqueous-phase emulsion or dispersion polymerization processes. The particle size distribution (PSD) of a latex is an important morphological characteristic because it modifies rheological, mechanical, and physical properties of materials such as adhesives, coatings, inks, or paints; as well as it affects some physico-chemical mechanisms (e.g., absorption, desorption, and termination of free radicals) that take place along heterogeneous polymerization reactions. For instance, particles with diameters close to the thickness of a coating can produce a streaky and non-uniform film; and the gloss, the hardness, and the drying time of a film depend on the PSD. Also, the stability of emulsions, dispersions, and suspensions decreases with the increase of the particle sizes and/or the PSD width [1–3].

Main definitions concerning latex PSDs were recently reviewed [4]. We shall call $f(D_i)$ the discrete number PSD and $w(D_i)$ the discrete weight PSD. The ordinates of $f(D_i)$ [or of $w(D_i)$] represent the number [or the weight] fractions of particles contained in the diameter interval $[D_i,\ D_{i+1}]$ $(i=1,\ 2,\ \ldots,\ \mathrm{N})$, which is regularly spaced at diameter intervals ΔD. Ordinates of $f(D_i)$ and $w(D_i)$ are related, through:

$$w(D_i) = \frac{\pi\rho}{6} D_i^3 f(D_i) \tag{1}$$

where ρ is the density of the polymer particles. On the basis of $w(D_i)$, the infinite average particle diameters can be defined through [4]:

$$\overline{D}_{a,b} = \left[\frac{\sum_{i=1}^{\mathrm{N}} w(D_i) D_i^{a-3}}{\sum_{i=1}^{\mathrm{N}} w(D_i) D_i^{b-3}} \right]^{\frac{1}{a-b}}, \quad (a, b\text{: integer numbers; } a > b) \tag{2}$$

Average diameters frequently reported are: the number–average diameter, $\overline{D}_{1,0}$; and the weight–average diameter, $\overline{D}_{4,3}$.

There are several techniques for sizing sub-micrometric polymer particles [4]. Dynamic light scattering (DLS) is an optical technique frequently used for estimating average diameters and PSDs of latexes.

* Corresponding author at: INTEC (CONICET and Universidad Nacional del Litoral), Güemes 3450 (3000) Santa Fe, Argentina. Tel.: +54 342 4511370; fax: +54 342 4511079.
E-mail addresses: laclementi@santafe-conicet.gov.ar (L.A. Clementi), jvega@santafe-conicet.gov.ar (J.R. Vega), lgug@intec.unl.edu.ar (L.M. Gugliotta), helcio@mecanica.ufrj.br (H.R.B. Orlande).

0169-7439/$ – see front matter © 2011 Elsevier B.V. All rights reserved.
doi:10.1016/j.chemolab.2011.03.003

In DLS, a dilute sample of a particulate system is irradiated with a monochromatic laser, and the particles scatter the light in all directions. Due to the Brownian motion of particles, the light scattered at any angle (θ_r) fluctuates along the time. At any given θ_r, the raw DLS measurement is the second-order autocorrelation function of the scattered light intensity, $G^{(2)}_{\theta_r}(\tau_j)$, where τ_j is the autocorrelation delay time. A mathematical model that describes the measurement process is summarized in the Appendix A.

A PSD can be estimated on the basis of a unique autocorrelation function $G^{(2)}_{\theta_0}(\tau_j)$ acquired at a single angle θ_0 [4,5], or alternatively from a set of $G^{(2)}_{\theta_r}(\tau_j)$ taken at different θ_r (multiangle DLS: MDLS) [6–10]. In any case, the estimation procedure involves the solution of an ill-conditioned linear inverse problem, where small noises present in the measurements lead to large changes in the estimated PSD. In general, the inverse problem for estimating the weight PSD is better conditioned than the inverse problem for estimating the number PSD [11]. Nowadays, several techniques are available for solving ill-conditioned inverse problems. Regularization techniques basically involve a least-squares minimization of the differences between the measurements and their predictions by a mathematical model, and try to improve the ill-conditioning of the inverse problem by including an adjustable regularization parameter and/or some a priori knowledge or smoothness conditions on the sought solution [12–16]. The widely-used CONTIN program [17] (originally implemented in FORTRAN and now available in the public domain) is often used for inverting ill-conditioned linear problems through a constrained regularization method, and was applied to invert MDLS autocorrelation functions [18].

For the MDLS model described in the Appendix A [see Eq. (A.6)], the well-known constrained Tikhonov regularization method [12] can be stated as:

$$\underset{\hat{\mathbf{w}}_\alpha}{Min}\ \left\{\left\|\mathbf{g}^{(1)}-\mathbf{F}\ \hat{\mathbf{w}}_\alpha\right\|^2+\alpha\left\|\mathbf{H}\ \hat{\mathbf{w}}_\alpha\right\|^2\right\};\quad \text{subject to } \hat{\mathbf{w}}_\alpha\geq 0 \tag{3}$$

where the symbol "^" stands for estimated value; the vector $\hat{\mathbf{w}}_\alpha$ contains the heights of the estimated PSD, $\hat{w}_\alpha(D_i)$; α is a regularization parameter; $\mathbf{H}$ is a regularization matrix (typically, the discrete second derivative operator); and $\|\cdot\|$ represents the 2-norm of a vector. Clearly, the solution of Eq. (3) will depend on the selected α. While a strong regularization (i.e., a large α) produces an excessively smoothened and wide PSD, a weak regularization normally originates an oscillatory PSD that tends to the least-squares solution when $\alpha\to 0$. Therefore, the user normally chooses a trade-off solution at an intermediate α. Some available algorithms for automatically determining α are the generalized cross-validation technique [19,20], and the L-curve method [20,21]. Regularization tools (coded as a MATLAB package) are available in the public domain [22], and are useful for inverting discrete ill-conditioned linear problems written in the form of Eq. (3).

The method of cumulants [23] can be applied onto $g^{(1)}_{\theta_r}(\tau_j)$ [see Appendix A] for calculating the angle-dependent average DLS diameters, $\overline{D}_{\mathrm{DLS}}(\theta_r)$. In general, none of these $\overline{D}_{\mathrm{DLS}}(\theta_r)$ will coincide with the $\overline{D}_{a,b}$ of Eq. (2). In contrast, the $\overline{D}_{\mathrm{DLS}}(\theta_r)$ are related to the PSD through the following relationship [6,24,25]:

$$\overline{D}_{\mathrm{DLS}}(\theta_r)=\frac{\sum_{i=1}^{N} C_I\left(\theta_r,D_i,n_p\right)w(D_i)/D_i^3}{\sum_{i=1}^{N} C_I\left(\theta_r,D_i,n_p\right)w(D_i)/D_i^4};\quad (r=1,\ldots,\mathrm{R}). \tag{4}$$

Then, the weight PSD, $w(D_i)$, can be estimated from the derived measurements, $\overline{D}_{\mathrm{DLS}}(\theta_r)$, by solving the ill-conditioned inverse problem of Eq. (4). Since Eq. (4) is non-linear, then the classical regularization techniques implemented in the CONTIN program [17] or in the Hansen's routines [22] can not directly be used for estimating the PSD. In contrast, the inversion of Eq. (4) presents the advantage of using $\overline{D}_{\mathrm{DLS}}(\theta_r)$, which normally exhibits a reduced level of noise with respect to the raw autocorrelations, as a consequence of the filtering effect introduced by the method of cumulants [23].

Some numerical methods for solving Eq. (4) have already been proposed [24,25]. In Ref. [24], bimodal PSDs were approximated by two single-spike modes, and each mode was estimated through a global-searching optimization algorithm. More recently, the problem was solved on the basis of general regression neural networks [25], but some drawbacks remain still present (e.g., the estimated PSD can strongly depend on the selected training patterns).

In the last years, statistical techniques based on Bayesian inference became useful tools for solving inverse problems. Bayesian inversion techniques consider both measurements and unknown parameters as random variables, and aim at estimating their probability density functions [26]. In practical applications, the so-called 'posterior probability density function' included in the Bayes' theorem can not be analytically derived or numerically computed in reasonable computing times. In such cases, Markov chain Monte Carlo (MCMC) methods are typically used to generate samples so that any statistical inference derived on the basis of such samples will coincide with the waited statistics in the sought posterior probability density function [27].

Bayesian methods have been applied to solve linear as well as non-linear inverse problems in several fields of science. Hibbert and Armstrong [28] published a review covering more than 200 articles on applications of Bayesian techniques to the analysis of chemistry data. Recently, a non-linear inverse problem of thermal characteristics was solved through a Bayesian-MCMC methodology that produced a good performance when tested on the basis of an experimental example [29]. Only a few publications utilized Bayesian inference for estimating PSDs. For example, the PSD of a ferrofluid was estimated from magnetization measurements through a Bayesian inversion method [30]. The inverse problem involved a model similar to that of Eq. (A.2); and the method produced acceptable results when tested on an experimental example. A complete study on the estimation of PSDs of ferrofluids from magnetization measurements and on the basis of Bayesian analysis was published in Ref. [31]. As far as the authors are aware, Bayesian methods have not yet been investigated for estimating PSDs of latex from MDLS measurements.

In this work, we propose the use of a Bayesian inference technique for solving the non-linear ill-conditioned inverse problem of estimating the weight PSD of a latex from their average diameters derived on the basis of MDLS measurements. The method is evaluated through simulated and experimental examples. All the estimated PSDs are compared with independent estimations obtained through the classical approach of inverting the measured autocorrelation functions with standard regularization techniques for ill-conditioned linear problems.

2. Measurement pre-processing and Bayesian inversion method

2.1. Measurement pre-processing

Assume first that R raw MDLS measurements, $G^{(2)}_{\theta_r}(\tau_j)$, are available ($r=1,\ldots,\mathrm{R}$). As schematically represented on the left side of Fig. 1, the pre-processing of $G^{(2)}_{\theta_r}(\tau_j)$ involves two steps: 1) the calculation of the R secondary measurements, $g^{(1)}_{\theta_r}(\tau_j)$, through Eq. (A.1); and 2) the calculation of the R average diameters, $\overline{D}_{\mathrm{DLS}}(\theta_r)$, by application of the method of cumulants [23] onto each $g^{(1)}_{\theta_r}(\tau_j)$. Due to the unavoidable measurement noises present in $G^{(2)}_{\theta_r}(\tau_j)$, the derived measurement $\overline{D}_{\mathrm{DLS}}(\theta_r)$ can be considered as a random variable.

2.2. The Bayesian inversion method

The weight PSD can be estimated by the numerical inversion of Eq. (4), from the knowledge of $\overline{D}_{\mathrm{DLS}}(\theta_r)$. Let us define vectors $\mathbf{w}$ and $\overline{\mathbf{D}}$

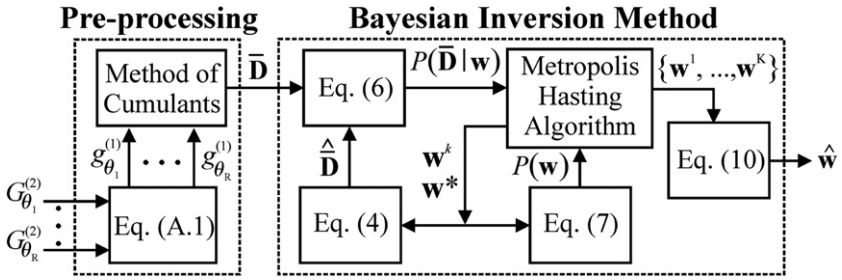

Fig. 1. The proposed method for estimating the PSD from the MDLS measurements. A schematic representation of the measurement pre-processing and the Bayesian inversion method.

as: $\mathbf{w}=[w(D_1),\ldots,\ w(D_N)]^T$ (i.e., the vector that contains the ordinates of the unknown weight PSD); and $\overline{\mathbf{D}}=\left[\overline{D}_{DLS}(\theta_1),\ldots,\ \overline{D}_{DLS}(\theta_R)\right]^T$ (i.e., the vector that contains the ordinates of the calculated average diameters). By considering $\mathbf{w}$ and $\overline{\mathbf{D}}$ as random variables, the Bayes' theorem can be stated as [27]:

$$P(\mathbf{w}|\overline{\mathbf{D}})=\frac{P(\overline{\mathbf{D}}|\mathbf{w})P(\mathbf{w})}{P(\overline{\mathbf{D}})} \tag{5}$$

where $P(\mathbf{w}|\overline{\mathbf{D}})$ is the posterior probability density function (i.e., the conditional probability of the unknown $\mathbf{w}$ given the measurements $\overline{\mathbf{D}}$); $P(\overline{\mathbf{D}}|\mathbf{w})$ is the likelihood function (i.e., the conditional probability of the measurements $\overline{\mathbf{D}}$ given the unknown $\mathbf{w}$); $P(\mathbf{w})$ is the prior probability density function (i.e., a statistical model for the unknown $\mathbf{w}$, which contains all the previous information available on the uncertain parameters, but without including the information conveyed by the new measurements); and $P(\overline{\mathbf{D}})$ is the marginal probability density of the measurements, which plays the role of a normalization constant.

We shall assume that the measurement errors, $\overline{\mathbf{D}}-\hat{\overline{\mathbf{D}}}$, are Gaussian random variables (of known means and covariances), additive, and independent of the unknowns. With these hypotheses, the likelihood function can be expressed as [29,30]:

$$P(\overline{\mathbf{D}}|\mathbf{w})=K_1\,e^{\left\{-\frac{1}{2}\left[\overline{\mathbf{D}}-\hat{\overline{\mathbf{D}}}\right]^T\mathbf{C}_D^{-1}\left[\overline{\mathbf{D}}-\hat{\overline{\mathbf{D}}}\right]\right\}} \tag{6}$$

where K_1 is a known constant that depends on the covariance matrix of the measurement errors, $\mathbf{C}_D$; and $\hat{\overline{\mathbf{D}}}$ is the average diameters obtained through Eq. (4) for a given PSD.

As prior information on the weight PSD, we assume that $w(D_i)$ should be a reasonable smooth and non-negative function; and among several possible smoothness conditions to be chosen, we particularly adopt that the PSD has finite second derivatives. These assumptions can be written in the form of a probability density function by using the maximum entropy principle [30], which leads to the following prior probability density function:

$$P(\mathbf{w})=\begin{cases}K_2\ e^{\left\{-\frac{1}{2}\gamma^2\mathbf{w}^T\mathbf{H}^T\mathbf{H}\mathbf{w}\right\}}; & \text{for } \mathbf{w}\geq 0\\ 0; & \text{otherwise}\end{cases} \tag{7}$$

where K_2 is a constant (that is strictly unnecessary for implementing the estimation procedure), and γ is a smoothing parameter that can be calculated by the L-curve method [20,21]. More detailed mathematical foundation concerning the selection of $P(\mathbf{w})$ can be consulted in Ref. [30].

By substituting Eqs. (6) and (7) into Eq. (5), we obtain:

$$P(\mathbf{w}|\overline{\mathbf{D}})=\begin{cases}\frac{K_1K_2}{P(\overline{\mathbf{D}})}e^{-\frac{1}{2}\left\{\left[\overline{\mathbf{D}}-\hat{\overline{\mathbf{D}}}\right]^T\mathbf{C}_D^{-1}\left[\overline{\mathbf{D}}-\hat{\overline{\mathbf{D}}}\right]+\gamma^2\mathbf{w}^T\mathbf{H}^T\mathbf{H}\mathbf{w}\right\}}; & \text{for } \mathbf{w}\geq 0\\ 0; & \text{otherwise}\end{cases} \tag{8}$$

On the basis of $P(\mathbf{w}|\overline{\mathbf{D}})$, it is possible to infer several PSD estimates (e.g., by selecting the mode, the mean, or an arbitrary moment of the distribution). In general, the evaluation of Eq. (8) requires to solve a high-dimension integration for calculating $P(\overline{\mathbf{D}})$, and the numerical procedure would be extremely time-consuming. To overcome such problem, a Markov chain Monte Carlo (MCMC) method is normally used for generating a sequence of random samples drawn from $P(\mathbf{w}|\overline{\mathbf{D}})$; and therefore statistical information on $P(\mathbf{w}|\overline{\mathbf{D}})$ can directly be inferred from the generated samples. Here, the MCMC method was implemented in the form of a Metropolis–Hasting algorithm [27,29].

2.2.1. Metropolis–Hasting algorithm

The Metropolis–Hasting algorithm is used to draw a sequence of random samples from $P(\mathbf{w}|\overline{\mathbf{D}})$. The algorithm can be summarized in the following steps [27,29]:

1. Start with any initial distribution $\mathbf{w}^1$ that satisfies $P(\mathbf{w}^1|\overline{\mathbf{D}})>0$. Set $k=1$.
2. Use the current $\mathbf{w}^k$ to obtain a new candidate $\mathbf{w}^*$, from some jumping distribution $q(\mathbf{w}^k,\ \mathbf{w}^*)$, which is the probability of returning $\mathbf{w}^*$ given $\mathbf{w}^k$.
3. Given the candidates $\mathbf{w}^k$ and $\mathbf{w}^*$, calculate the acceptance factor:

$$\xi=\ min\left[1,\frac{P(\mathbf{w}^*|\overline{\mathbf{D}})\ q\left(\mathbf{w}^k,\mathbf{w}^*\right)}{P(\mathbf{w}^k|\overline{\mathbf{D}})\ q(\mathbf{w}^*,\mathbf{w}^k)}\right]=\ min\left[1,\frac{P(\mathbf{w}^*)\ P(\overline{\mathbf{D}}|\mathbf{w}^*)\ q\left(\mathbf{w}^k,\mathbf{w}^*\right)}{P(\mathbf{w}^k)\ P(\overline{\mathbf{D}}|\mathbf{w}^k)\ q(\mathbf{w}^*,\mathbf{w}^k)}\right] \tag{9}$$

4. Choose a random value U from a uniform distribution on (0,1). If $U\leq\xi$, set $\mathbf{w}^{k+1}=\mathbf{w}^*$; otherwise, $\mathbf{w}^{k+1}=\mathbf{w}^k$.
5. Set $k=k+1$ and return to step 2 in order to generate the sequence $\{\mathbf{w}^1,\ldots,\mathbf{w}^k\}$.

This iterative procedure generates a Markov chain $\{\mathbf{w}^1,\ldots,\mathbf{w}^K\}$, provided that the transition probabilities from $\mathbf{w}^k$ to $\mathbf{w}^{k+1}$ depends only on $\mathbf{w}^k$ and not on $\{\mathbf{w}^1,\ldots,\mathbf{w}^{k-1}\}$. After a sufficiently large burn-in period (of B iterations), the chain reaches its stationary distribution, and the set $\{\mathbf{w}^{B+1},\ldots,\mathbf{w}^K\}$ are samples from $P(\mathbf{w}|\overline{\mathbf{D}})$.

2.2.2. Estimation of the PSD

After simulating several arbitrary examples, we found that the mean of $P(\mathbf{w}|\overline{\mathbf{D}})$ produced better PSD estimates than the mode or

other $P(\mathbf{w}|\overline{\mathbf{D}})$ moments. Accordingly, the PSD estimate $\hat{\mathbf{w}}$ can be calculated from the stationary Markov chain $\{\mathbf{w}^{B+1},\ldots,\mathbf{w}^{K}\}$, as follows:

$$\hat{\mathbf{w}} = \frac{\sum_{i=B+1}^{K} \mathbf{w}^i}{(K-B)}. \quad (10)$$

The Bayesian procedure is schematically described on the right side of Fig. 1.

3. Validation of the proposed method

Simulated (or "synthetic") examples were implemented for validating the proposed estimation method. In all cases, the procedure for obtaining the synthetic MDLS measurements basically involved the following steps: (i) definition of an arbitrary PSD; (ii) simulation of the (noise-free) measurements, $G^{(2)}_{\theta_r}(\tau_j)$, through the mathematical model described in the Appendix A; and (iii) calculation of the noisy measurements, $\tilde{G}^{(2)}_{\theta_r}(\tau_j)$, by addition of typical noises to $G^{(2)}_{\theta_r}(\tau_j)$.

In what follows, we will apply the above-commented procedure to two weight PSDs corresponding to hypothetical polystyrene (PS) latexes, with spherical particles of diameters in the range [200–550] nm, regularly spaced each $\Delta D = 1$ nm. The number PSDs, $f(D_i)$, were initially defined according to shapes normally used in the literature [6,25]; and then transformed into weight PSDs through Eq. (1).

The first number PSD, $f_1(D_i)$, was a highly asymmetric exponentially-modified Gaussian (EMG) distribution, which was obtained by convoluting a Gaussian distribution (of mean diameter $\overline{D}_G = 340$ nm, and standard deviation $\sigma_G = 10$ nm), with a decreasing exponential function (of decay constant $D_0 = 20$ nm). Then, the weight PSD, $w_1(D_i)$, was:

$$w_1(D_i) = \frac{\pi^{1/2} D_i^3 \rho \Delta D}{6\sqrt{2}\sigma_G} \exp\left[-\frac{(D_i-\overline{D}_G)^2}{2\ \sigma_G^2}\right] * \frac{\exp(-D_i/D_0)}{D_0/\Delta D}; \quad (i = 1,\ldots,N) \quad (11)$$

where the symbol '*' represents the convolution product.

The second number PSD, $f_2(D_i)$, was a bimodal distribution obtained by combining two log-normal distributions, $f_{2,1}(D_i)$ and $f_{2,2}(D_i)$; with the parameters of each mode selected as: $\overline{D}_{g,1} = 300$ nm, $\sigma_{L,1} = 0.10$, for $f_{2,1}$; and $\overline{D}_{g,2} = 425$ nm, $\sigma_{L,2} = 0.04$, for $f_{2,2}$. The relative masses of particles in each mode were: 8% and 92% (that correspond to number fractions of 20% and 80%, respectively). Then, the weight PSD was obtained through:

$$w_2(D_i) = \frac{D_i^2 \rho \Delta D}{6\sqrt{2}\pi^{-1/2}} \left\{ \frac{0.2}{\sigma_{L,1}} \exp\left[\frac{-\left[\ln(D_i/\overline{D}_{g,1})\right]^2}{2\sigma_{L,1}^2}\right] + \frac{0.8}{\sigma_{L,2}} \exp\left[\frac{-\left[\ln(D_i/\overline{D}_{g,2})\right]^2}{2\sigma_{L,2}^2}\right] \right\}; \quad (i = 1,\ldots,N). \quad (12)$$

Distributions w_1 and w_2 exhibit different shapes, peak variances, and asymmetries, and were selected to evaluate the capability of the proposed method to discriminate among the different kinds of PSDs. While w_1 exhibits a single peak with a highly asymmetric right tail, w_2 is a bimodal PSD, where the mass-concentration of the smaller particles is lower than the mass-concentration of the bigger ones.

Simulation of the light scattering processes assumed a constant temperature of 30 °C ($T = 303.15$ K) and a vertically-polarized He–Ne laser of wavelength $\lambda = 632.8$ nm. At this λ, the refractive indexes were: $n_p = 1.5729$, for the PS particles [32]; and $n_m = 1.3319$, for the dispersion medium (pure water). The measurement angles were selected at regular intervals of 10°, in the range [30°–140°]; i.e. $R = 12$. These parameters were used to evaluate the coefficient $C_l(\theta_r, D_i, n_p)$ through the Mie scattering theory [33,34], and are required to simulate the noise-free measurements $G^{(2)}_{\theta_r}(\tau_j)$ through Eqs. (A.1)–(A.3). The noisy autocorrelation measurements, $\tilde{G}^{(2)}_{\theta_r}(\tau_j)$, were simulated by contaminating $G^{(2)}_{\theta_r}(\tau_j)$ with additive noises similar to those observed in experiments, as follows:

$$\tilde{G}^{(2)}_{\theta_r}(\tau_j) = G^{(2)}_{\theta_r}(\tau_j) + 0.001\ G^{(2)}_{\infty,\theta_r}\ \varepsilon; \quad (r = 1,\ldots,R), \quad (j = 1,\ldots,M) \quad (13)$$

where the baseline $G^{(2)}_{\infty,\theta_r}$ was calculated as detailed in Ref. [6]; and ε is a Gaussian random sequence of mean zero and variance one. For

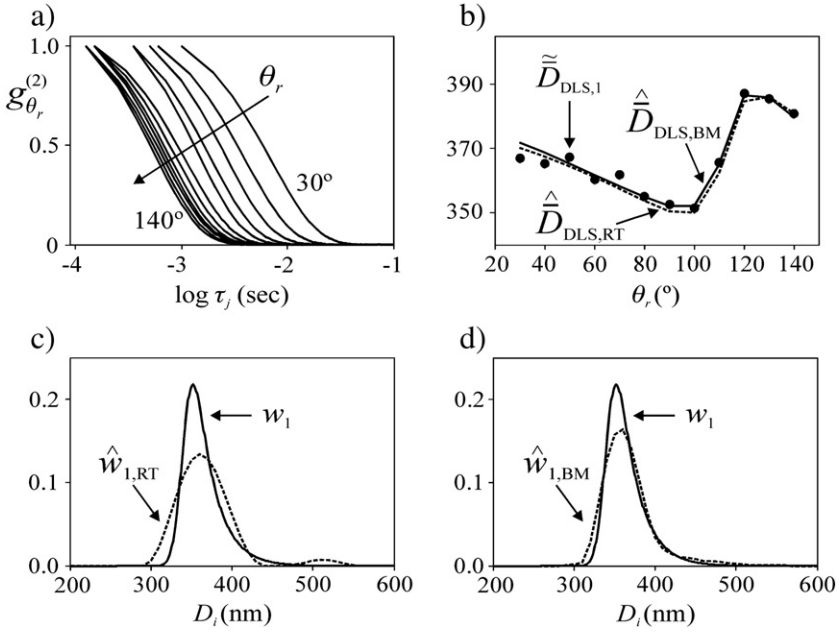

Fig. 2. Simulated example: unimodal PSD, w_1. (a) Normalized MDLS autocorrelations. (b) Average DLS diameters (in dots) obtained by pre-processing the MDLS measurements, and their simulated values from the estimated PSDs. (c, d) The simulated PSD and its estimates through RT (c) and BM (d).

a clearer visualization of the measurements, the autocorrelation functions were normalized according to [see Figs. 2a and 3a]: $g^{(2)}_{\theta_r}(\tau_j) = \left[\tilde{G}^{(2)}_{\theta_r}(\tau_j) - G^{(2)}_{\infty,\theta_r}\right] / \left[\tilde{G}^{(2)}_{\theta_r}(0) - G^{(2)}_{\infty,\theta_r}\right]$.

To implement the PSD estimation procedure, a diameter axis with N = 101 evenly-spaced points in the range [100–1100] nm was selected. To ensure an acceptable signal-to-noise ratios, each autocorrelation function was limited to its first thirty points (i.e., M = 30 for all θ_r). From $\tilde{G}^{(2)}_{\theta_r}(\tau_j)$, the noisy "measurements" $\tilde{\bar{D}}_{\mathrm{DLS}}(\theta_r)$ were obtained through the data pre-processing strategy of Fig. 1, and are represented by dots in Figs. 2b and 3b). In order to evaluate $\mathbf{C}_D$ [in Eq. (6)], hundreds of simulations of the described method were applied on arbitrary PSDs, and the standard deviations observed in $\tilde{\bar{D}}_{\mathrm{DLS}}(\theta_r)$ were adjusted through the following expression: $\tilde{\sigma}_r = 0.0025\ \mathrm{mean}\{\tilde{\bar{D}}_{\mathrm{DLS}}(\theta_r)\}$. At different angles, all measurements were assumed to be uncorrelated; and for this reason the covariance matrix, $\mathbf{C}_D$, was diagonal, i.e.: $\mathbf{C}_D = \mathrm{diag}\left(\tilde{\sigma}^2_1, \cdots, \tilde{\sigma}^2_R\right)$. The smoothness parameter γ in Eq. (7) was automatically selected according to the L-curve method [20,21].

In general, the Bayesian method (BM) would never assign a zero probability to an ordinate $w(D_i)$. Therefore, in the diameter ranges where the true PSD ordinates are zero, the estimated PSD ordinates would always exhibit small positive values (more than two orders of magnitude lower than the main modes, in the simulated examples). To preclude the presence of such unlikely nonzero ordinates, values of $\hat{w}(D_i)$ below a threshold of 0.5% of the PSD maximum were directly set to zero.

The Metropolis–Hasting algorithm was initialized with positive random values ($\mathbf{w}^1$) selected from a uniform distribution. The jumping distribution [$q(\mathbf{w}^k, \mathbf{w}^*)$] was selected as a Gaussian of zero mean and standard deviation of 0.001, which was adjusted by trial-and-error until reaching an acceptance rate close to 50% [27]. After several tests aimed at obtaining repetitive PSD estimates, the length of the Markov chain was set to 500,000 (much shorter lengths produced erratic estimates). The evolution of $P(\mathbf{w}|\overline{\mathbf{D}})$ corresponding to the example of the PSD w_1 is shown in Fig. 4 for the first 100,000 states (a similar evolution was also obtained for w_2). Fig. 4 reveals that the Markov chain reached its stationary state in a burn-in period of around 25,000 states.

The Bayesian inversion method produced the PSD estimates indicated by the subscript "BM" in Figs. 2d and 3d). Instead of $w(D_i)$, note that Fig. 3d) shows the number PSD, $f(D_i)$, to have a better visualization of the different modes.

In order to compare the ability of the proposed BM for estimating the PSD from MDLS measurements, the same numerical examples were solved through an independent method that is typically used for inverting ill-conditioned linear problems. To this effect, measurements $\tilde{G}^{(2)}_{\theta_r}(\tau_j)$ were arranged and processed according to the MDLS data treatment procedure described in Ref. [6]; and the corresponding inverse problem [Eq. (3)] was solved through a linear-constrained regularization technique (RT) implemented on the basis of the inversion tools reported by Hansen [22], with automatic selection of the regularization parameter α according to the L-curve method [20,21]. The obtained PSD estimates are indicated by the subscript "RT" in Figs. 2c and 3c). Note that Fig. 3c) also shows the number PSD, to highlight the estimation errors at the lower diameters.

The PSD estimates obtained by BM and RT were injected into Eq. (4) to simulate the "measured" average diameters, $\hat{\bar{D}}_{\mathrm{DLS}}(\theta_r)$, which are indicated by curves in Figs. 2b and 3b). The following indexes were defined to evaluate the performance of the estimations methods:

$$J_w = \left(\frac{\sum_{i=1}^{N} [w(D_i) - \hat{w}(D_i)]^2}{\sum_{i=1}^{N} [w(D_i)]^2} \right)^{0.5} \tag{14a}$$

$$J_D = \frac{1}{R} \left(\sum_{r=1}^{R} \left[1 - \frac{\hat{\bar{D}}_{\mathrm{DLS}}(\theta_r)}{\bar{D}_{\mathrm{DLS}}(\theta_r)} \right]^2 \right)^{0.5} \tag{14b}$$

$$J_g = \frac{1}{R\,M} \left(\sum_{r=1}^{R} \sum_{j=1}^{M} \left[g^{(1)}_{\theta_r}(\tau_j) - \hat{g}^{(1)}_{\theta_r}(\tau_j) \right]^2 \right)^{0.5} \tag{14c}$$

Index J_w can only be calculated when the true PSD is a priori known (e.g., in the case of simulated examples), and evaluates the differences between the true and the estimated PSDs. In contrast, indexes J_D and J_g can always be computed, and account for the method ability for recuperating the measurements. Note that: (i) J_w is the most representative performance index for evaluating the quality of a PSD

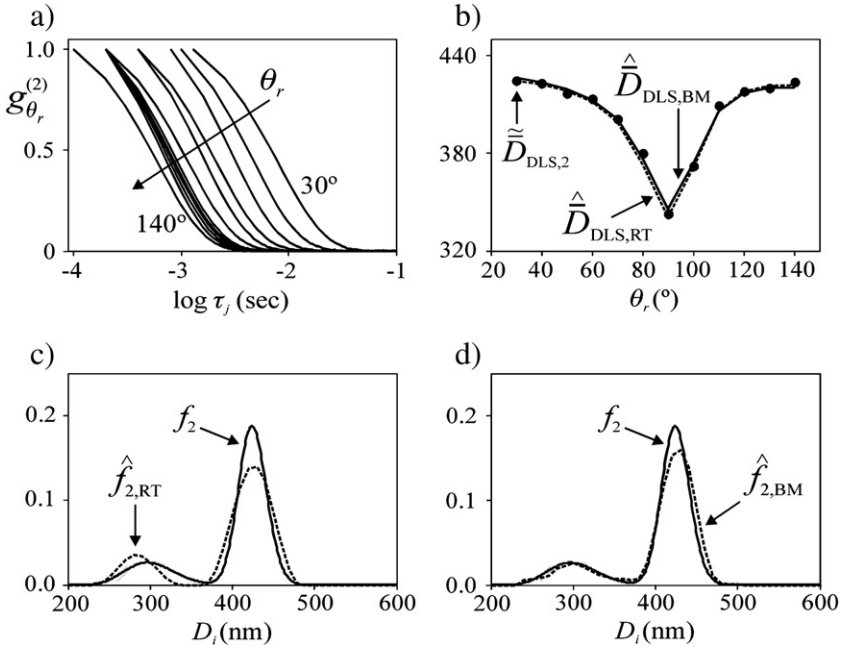

Fig. 3. Simulated example: bimodal PSD, w_2. Legends as in Fig. 2.

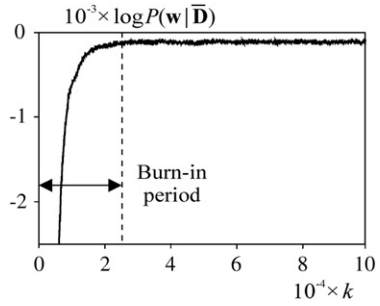

Fig. 4. Evolution of the posterior probability density function (in logarithmic scale), along the first 100,000 iterations, for the simulated unimodal PSD, w_1. The dashed vertical line indicates that the Markov chain reached its stationary state.

estimate; (ii) the BM is based on Eq. (4), and then will tend to minimize J_D; and (iii) the RT is based on Eq. (3), and then will tend to minimize J_g.

For all the PSD estimates, Table 1 shows the average diameters, $\overline{D}_{1,0}$ and $\overline{D}_{4,3}$, and the performance indexes of Eqs. (14a, 14b and 14c). In general, the BM produced better PSD estimates than the RT (in the sense of yielding lower J_w). As expected, the lower J_D also correspond to the BM, and the lower J_g correspond to the RT. In the case of the unimodal PSD w_1, the RT produced a broader PSD estimate and a spurious additional mode [Fig. 2c)]. The increase in the PSD width is attributed to the relatively strong regularization utilized to compensate for the measurement noises. The erroneous additional mode observed at 510 nm was impossible to be eliminated (even after applying stronger regularizations); and its effect on $\overline{D}_{\mathrm{DLS}}(\theta_r)$ is similar to the effect caused by the right tail of w_1. On the other hand, predictions through the BM seem to be less influenced by the measurement noises, and produced an acceptable PSD estimate. While RT was unable to estimate the asymmetry in w_1, the BM reasonably predicted the asymmetric right tail.

In the case of the bimodal PSD, w_2, both methods predicted the two modes, but the BM yielded a PSD estimate closer to the true one (see the lower J_w in Table 1, for each mode). While the BM produced an estimation that almost coincided with the simulated one, the RT estimated a too narrow smaller mode and with a slightly lower average diameter. Again, the expected tendencies for J_D and J_g are observed.

Consider some particular issues concerning the above-described comparison between BM and RT. While the proposed BM utilized the average diameters derived from the autocorrelations and then solved the non-linear inverse problem of Eq. (4), the selected RT was directly used to process the measured autocorrelations through a classical inversion method for linear problems (the Hansen's routines). In spite of the mentioned differences, a fair comparison of the performance of both methods can still be made under the following two main ideas: (i) the same raw measurements (i.e., the noisy autocorrelation functions) are used; and (ii) the key performance index J_w is an absolute measure of the errors between a true PSD and its estimates from each individual method. As previously stated, Eq. (4) is non linear and therefore it can not be solved through the classical routines. On the other hand, in this work the BM was disregarded as a reliable tool for inverting the complete set of autocorrelation functions because the advantages of the filtering implicit in the $\overline{D}_{\mathrm{DLS}}(\theta_r)$ measurements would be missing, and therefore a rather deteriorated PSD estimates would be expected.

All routines for the simulation of the light scattering processes as well as for the numerical solution of the inverse problems were coded in MATLAB (MathWorks™). In an Intel Core Duo processor, the numerical inversions involved typical computing times of around 80 s for either BM or RT.

Table 1
Simulated examples. Average diameters and performance indexes for the two analyzed PSDs. For the bimodal PSD (w_2), $\overline{D}_{1,0}$, $\overline{D}_{4,3}$, and J_w were evaluated for each mode.

	$w_1(D_i)$	$\hat{w}_1(D_i)$		$w_{2,1}/w_{2,2}$	$\hat{w}_{2,1}/\hat{w}_{2,2}$	
		BM	RT		BM	RT
$\overline{D}_{1,0}$ (nm)	360	360	358	301 / 425	303 / 427	285 / 426
$\overline{D}_{4,3}$ (nm)	365	367	367	309 / 427	313 / 430	289 / 429
$10^1\times J_w$ (−)	–	1.9	3.4	–	1.8 / 1.9	6.9 / 2.5
$10^3\times J_D$ (−)	–	1.7	1.9	–	1.6	2.0
$10^3\times J_g$ (−)	–	1.6	0.8	–	3.3	1.0

4. Application to experimental data

The BM was applied to estimate the PSD of 2 bimodal latexes (L_1 and L_2), which were obtained by mixing 2 PS standards (Polysciences, Inc.), of nominal diameters 300 nm and 1000 nm. For each latex, the weight fractions of the modes were gravimetrically determined, yielding: $\omega_{L1,1}$ $(=1-\omega_{L1,2})\approx 75\%$ and $\omega_{L2,1}$ $(=1-\omega_{L2,2})\approx 59\%$ (subscripts "1" and "2" refer to the smaller and larger particles, respectively). In general, the bimodal PSDs that involve narrow peaks of quite different magnitude and placed in a wide range of possible diameters are difficult to be estimated. In this sense, the investigated examples are important to check the capability of the proposed algorithm for estimating the number of predicted modes, as well as the average diameters and the weight fractions of each mode.

MDLS measurements were acquired with a general-purpose laser light-scattering photometer (Brookhaven Instruments, Inc.), fitted with a vertically-polarized He–Ne laser ($\lambda=632.8$ nm), and a digital correlator (model BI-2000 AT). All latexes were well diluted in distilled, filtered, and deionized water, and yield average light intensities lower than 200,000 counts/s at each detection angle, as recommended to avoid multiple scattering [6]. The measurements were carried out at 30 °C ($T=303.15$ K). The total measurement times ranged from 200 s to 500 s. The latexes were measured at the following nine detection angles ($R=9$): [30°, 40°, 50°, 60°, 70°, 80°, 90°, 110°, and 130°]. The normalized measured autocorrelation functions $g^{(2)}_{\theta_r}(\tau_j)$ are represented in Figs. 5a and 6a). Since at higher angles the raw autocorrelation functions are practically overlapped, then the measurements at 100°, 120°, and 140° were not implemented.

As in the cases of the simulated examples, a linear diameter axis with $N=101$ points was selected in the range [100–1100] nm; and all the measured autocorrelation functions were limited to their first $M=30$ points. The DLS average diameters, $\overline{D}_{\mathrm{DLS,meas.}}(\theta_r)$, were obtained by pre-processing the raw measurements, and are represented by dots in Figs. 5b) and 6b). These values were fed into the proposed BM for estimating the PSDs of latexes L_1 and L_2; and the resulting PSD estimates are indicated by $\hat{w}_{\mathrm{L1,BM}}$ and $\hat{w}_{\mathrm{L2,BM}}$, in Figs. 5d and 6d). For comparison, the RT was also used to estimate the PSDs of both latexes from the measured $G^{(2)}_{\theta_r}(\tau_j)$. The resulting PSD estimates are indicated by $\hat{w}_{\mathrm{L1,RT}}$ and $\hat{w}_{\mathrm{L2,RT}}$, in Figs. 5c and 6c).

For evaluating the performance of each method, reference PSDs must be adopted for latex L_1 and L_2. These PSDs were obtained on the basis of the specifications of each standard, as provided by the manufacturer from disk centrifuge (DC) measurements [4], and weighted according to the mixing proportions used during the latex preparation. For each standard, the reported average diameter and standard deviations were: $D_{\mathrm{PS1}}=306$ nm, $D_{\mathrm{PS2}}=974$ nm, $\sigma_{\mathrm{PS1}}=8$ nm, and $\sigma_{\mathrm{PS2}}=10$ nm. Then, the reference PSDs were represented by bimodal distributions with Gaussian modes centered at the diameters D_{PS1} and D_{PS2}, with standards deviations σ_{PS1} and σ_{PS2}. The heights of the modes were scaled according to their weight fractions as follows: $\omega_{L1,1}=75\%$ and $\omega_{L1,2}=25\%$, for the first and second mode of latex L_1; and $\omega_{L2,1}=59\%$ and $\omega_{L2,2}=41\%$, for the first and second mode of latex L_2. Figs. 5b and 6b) show the average diameters obtained by injecting the reference PSDs into Eq. (4), which considerably differ from the measured $\overline{D}_{\mathrm{DLS,meas.}}(\theta_r)$, especially at higher angles. This might be due to small errors in the characterizations of the standards as well as in the experimental determinations of the weight fractions corresponding to both latexes.

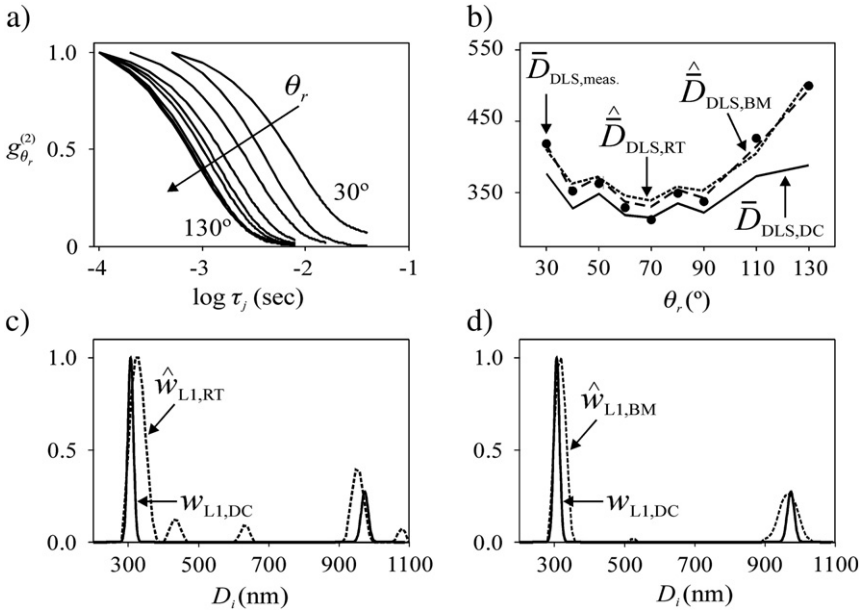

Fig. 5. Experimental example: Latex L1. (a) Normalized MDLS autocorrelations. (b) Average DLS diameters (in dots) obtained by pre-processing the MDLS measurements, and their simulated values from the estimated PSDs. (c, d) The reference PSD obtained by the disk centrifuge (DC) technique, and its estimates through RT (c) and BM (d).

Table 2 (for latex L1) and Table 3 (for latex L2) show the average diameters $\overline{D}_{1,0}$ and $\overline{D}_{4,3}$, the weight fractions, and the performance indexes calculated for the reference and the estimated PSDs. Again, the BM produced better estimations (lower J_w) than RT, and it was able to acceptably estimate the average diameters and the weight fractions of each mode. Figs. 5c and 6c) show that the RT predicted several spurious modes. In the case of latex L1, the BM also produced an erroneous mode around 500 nm (almost imperceptible in Fig. 5d), with a weight fraction lower than 1%. This mode remained present because it was higher than the adopted threshold of 0.5%.

5. Conclusions

An inversion method for estimating multimodal PSDs of polymeric latexes from MDLS measurements was developed on the basis of a Bayesian inference strategy. While classical RTs normally solve an optimization linear problem that consists in numerically inverting a Fredholm equation from the autocorrelation measurements, the proposed BM solves a nonlinear optimization problem that consists in inverting the light scattering model [included in Eq. (4)] from the MDLS average diameters. Such diameters are obtained after a straightforward pre-processing of the measured autocorrelations.

The proposed BM aimed at minimizing the errors between the measured and simulated average diameters, and for this reason produced more reduced J_D. In contrast, classical RTs are designed to minimize the differences between measured and simulated autocorrelation functions, thus yielding lower J_g. When evaluated through simulated and experimental examples, the BM produced improved PSDs (lower J_w) with respect to RT. This can probably be due to the

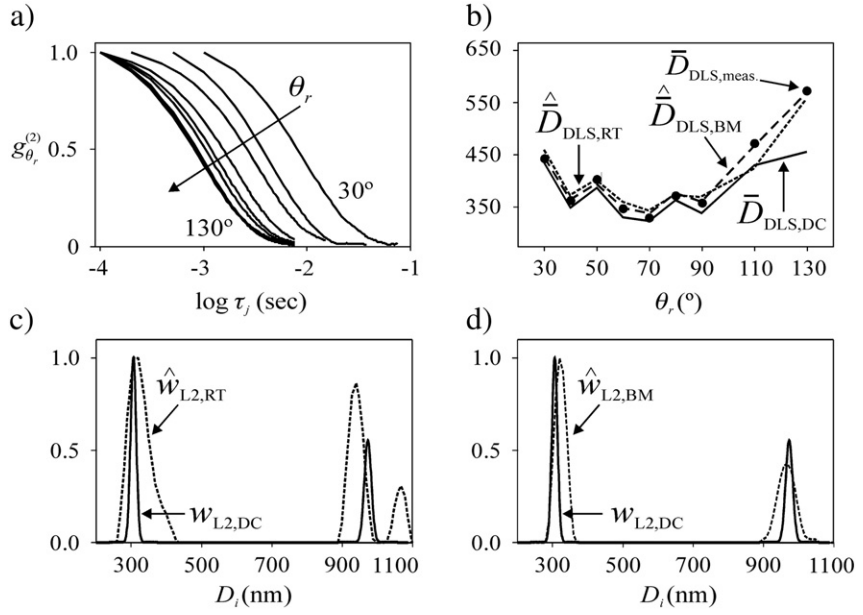

Fig. 6. Experimental example: Latex L2. Legends as in Fig. 5.

Table 2
Experimental example (PS latex L1). Average diameters, weight particle fractions, and performance indexes ($\overline{D}_{1,0}$, $\overline{D}_{4,3}$, $\hat{\omega}_1$, $\hat{\omega}_2$, and J_w were evaluated for each mode).

	Reference PSD	Estimated PSDs	
		BM	RT
$\overline{D}_{1,0}$ (nm)	306 / 974	315 / 966	324 / 954
$\overline{D}_{4,3}$ (nm)	307 / 974	317 / 968	327 / 955
$\hat{\omega}_1$ / $\hat{\omega}_2$ (%)	75 / 25	70 / 29	68 / 21
$10^1 \times J_w$ (−)	–	8.6 / 9.6	12.7 / 10.7
$10^3 \times J_D$ (−)	–	8.3	14.4
$10^3 \times J_g$ (−)	–	4.8	0.9

fact that the calculated average diameters were less affected by the noises present in the measured autocorrelations, and therefore BM requires a lower level of regularization than RT.

In general, the RT produced spurious modes in the estimated PSDs. Such artifacts could be eliminated through a stronger regularization, but would lead to extremely broad PSD estimates. On the other hand, the crude application of the BM always predicts nonzero PSD estimates along the diameter axis (with an appearance similar to a positive noise close to zero), because from a statistical point of view nonzero PSD ordinates always have some chance to occur. However, such unreal predictions were successfully suppressed by adequately selecting a minimum threshold below which all ordinates are considered to be zero. In this way, BM produced no meaningful spurious mode in the PSD estimates.

Though not presented in this paper, several other PSDs were also analyzed through BM and RT. In the cases of almost-symmetric unimodal and broad PSDs, as well as for PSDs including large particles (e.g., with diameters close to 1 μ), both methods produced accurate PSD estimates. For PSD modes that included particles with diameters lower than 100 nm, both methods yielded erroneous predictions. This is attributed to the fact that scattering produced by small particles (scattering in the Rayleigh regime) is identical at all angles, and therefore MDLS has no meaningful additional advantage on a single-angle DLS.

Acknowledgements

The authors are grateful for financial support received from CONICET, MinCyT, Universidad Nacional del Litoral, Universidad Tecnológica Nacional (Argentina), and CNPq — Project 490.556/2007-8 of the Program PROSUL (Brazil).

Appendix A

Mathematical model for multiangle DLS measurements

In DLS, a digital correlator measures the second-order autocorrelation function of the light scattered at a given θ_r, $G^{(2)}_{\theta_r}(\tau_j)$, for different values of the time delay, τ_j ($j=1, \ldots, M$). In MDLS, several measurements are collected at different θ_r ($r=1, \ldots, R$); and each $G^{(2)}_{\theta_r}(\tau_j)$ is related to its corresponding (first-order and normalized) autocorrelation function of the electric field, $g^{(1)}_{\theta_r}(\tau_j)$, through [6]:

$$G^{(2)}_{\theta_r}\left(\tau_j\right) = G^{(2)}_{\infty,\theta_r}\left[1 + \beta\left(g^{(1)}_{\theta_r}\left(\tau_j\right)\right)^2\right]; \quad (r = 1, \ldots, R), \quad (j = 1, \ldots, M) \tag{A.1}$$

where $G^{(2)}_{\infty,\theta_r}$ is the measured baseline; β (<1) is an instrumental parameter; and M is the number of points of each autocorrelation function. At a given θ_r, $g^{(1)}_{\theta_r}(\tau_j)$ is related to $w(D_i)$ as follows [6]:

$$g^{(1)}_{\theta_r}\left(\tau_j\right) = k_{\theta_r} \sum_{i=1}^{N} e^{-\frac{\Gamma_0(\theta_r)\tau_j}{D_i}} \frac{C_I\left(\theta_r, D_i, n_p\right)}{D_i^3} w(D_i); \quad (r = 1, \ldots, R), \quad (j = 1, \ldots, M) \tag{A.2}$$

with:

$$\Gamma_0(\theta_r) = \frac{16\pi}{3}\left(\frac{n_m}{\lambda}\right)^2 \frac{k_B T}{\eta} \sin^2(\theta_r/2); \quad (r = 1, \ldots, R) \tag{A.3}$$

where k_{θ_r} are (a priori unknown) proportionality constants that adopt different values at different θ_r; C_I is the fraction of light intensity scattered at θ_r by a single particle of diameter D_i and refractive index n_p; λ is the in-vacuo wavelength of the incident laser light; n_m is the refractive index of the non-absorbing medium; k_B is the Boltzmann's constant; T is the absolute temperature; and η is the medium viscosity at T. The key coefficient $C_I(\theta_r, D_i, n_p)$ in Eq. (A.2) additionally depends on λ and on the laser light polarization, and can be calculated through the Mie scattering theory [33,34]. The constants k_{θ_r} can be seen as normalization factors that insure $g^{(1)}_{\theta_r}(0) = 1$ [6].

In vector notation, (A.2) can be rewritten in the following linear form:

$$\mathbf{g}^{(1)}_{\theta_r} = k_{\theta_r}\mathbf{F}_{\theta_r}\mathbf{w}; \quad (r = 1, \ldots, R) \tag{A.4}$$

where the vectors $\mathbf{g}^{(1)}_{\theta_r}$ (M×1) and $\mathbf{w}$ (N×1) contain the discrete heights of $g^{(1)}_{\theta_r}(\tau_j)$ and $w(D_i)$, respectively, and $\mathbf{F}_{\theta_r}$ (M×N) is a kernel matrix corresponding to the DLS measurement at θ_r. The elements of $\mathbf{F}_{\theta_r}$ are given by [see Eq. (A.2)]:

$$F_{\theta_r}(j,i) = e^{-\frac{\Gamma_0(\theta_r)\tau_j}{D_i}} \frac{C_I\left(\theta_r, D_i, n_p\right)}{D_i^3}; \quad (i = 1, \ldots, N); \quad (j = 1, \ldots, M); \quad (r = 1, \ldots, R). \tag{A.5}$$

In a more general vector notation, the MDLS problem of Eq. (A.4) can be written as:

$$\mathbf{g}^{(1)} = \begin{bmatrix} \mathbf{g}^{(1)}_{\theta_1} \\ \vdots \\ \mathbf{g}^{(1)}_{\theta_R} \end{bmatrix} = \begin{bmatrix} k_{\theta_1}\mathbf{F}_{\theta_1} \\ \vdots \\ k_{\theta_R}\mathbf{F}_{\theta_R} \end{bmatrix} \mathbf{w} = \mathbf{F}\mathbf{w}. \tag{A.6}$$

Table 3
Experimental example (PS latex L2). Average diameters, weight particle fractions, and performance indexes ($\overline{D}_{1,0}$, $\overline{D}_{4,3}$, $\hat{\omega}_1$, $\hat{\omega}_2$, and J_w were evaluated for each mode).

	Reference PSD	Estimated PSDs	
		BM	RT
$\overline{D}_{1,0}$ (nm)	306 / 974	320 / 966	319 / 939
$\overline{D}_{4,3}$ (nm)	307 / 974	323 / 968	327 / 940
$\hat{\omega}_1$ / $\hat{\omega}_2$ (%)	59 / 41	61 / 39	57 / 33
$10^1 \times J_w$ (−)	–	10.9 / 9.1	13.5 / 14.4
$10^3 \times J_D$ (−)	–	4.6	14.7
$10^3 \times J_g$ (−)	–	5.3	1.2

References

[1] E.A. Collins, Measurement of particle size and particle size distribution, in: P.A. Lovell, M.S. El-Aasser (Eds.), Emulsion Polymerization and Emulsion Polymers, J. Wiley and Sons, Chichester, U.K, 1997, pp. 385–436.
[2] D. Urban, K. Takamura, Polymer Dispersions and Their Industrial Applications, Wiley-VCH, Weinheim, 2002.
[3] M. Barandiaran, J.C. de la Cal, J.M. Asua, Emulsion polymerization, in: J.M. Asua (Ed.), Polymer Reaction Engineering, Blackwell Pub, Oxford, 2007, pp. 233–272.
[4] L.M. Gugliotta, L.A. Clementi, J.R. Vega, Particle size distribution. main definitions and measurement techniques, in: L.M. Gugliotta, J.R. Vega (Eds.), Measurement of Particle Size Distribution of Polymer Latexes, Research Signpost — Transworld Research Network, Kerala, India, 2010, pp. 1–58.
[5] L.M. Gugliotta, J.R. Vega, G.R. Meira, Latex particle size distribution by dynamic light scattering: computer evaluation of two alternative calculation paths, J. Colloid Interface Sci. 228 (2000) 14–17.

[6] J.R. Vega, L.M. Gugliotta, V.D.G. Gonzalez, G.R. Meira, Latex particle size distribution by dynamic light scattering. A novel data processing for multi-angle measurements, J. Colloid Interface Sci. 261 (2003) 74–81.
[7] P.G. Cummins, E.J. Staples, Particle size distributions determined by a multiangle analysis of photon correlation spectroscopy data, Langmuir 3 (1987) 1109–1113.
[8] S.E. Bott, Enhanced resolution particle size distributions by multiple angle photon correlation spectroscopy, in: P.J. Lloyd (Ed.), Particle Size Analysis, J. Wiley & Sons, Washington D.C., 1988, pp. 77–88.
[9] G. Bryant, J. Thomas, Improved particle size distribution measurements using multiangle dynamic light scattering, Langmuir 11 (1995) 2480–2485.
[10] G. Bryant, C. Abeynayake, J. Thomas, Improved particle size distribution measurements using multiangle dynamic light scattering. 2. Refinements and applications, Langmuir 12 (1996) 6224–6228.
[11] C. De Vos, L. Deriemaeker, R. Finsy, Quantitative assessment of the conditioning of the inversion of quasi-elastic and static light scattering data for particle size distribution, Langmuir 12 (1996) 2630–2636.
[12] A.N. Tikhonov, V. Arsenin, Solution of Ill-posed Problems, Wiley, New York, 1977.
[13] A. Kirsch, Introduction to the Mathematical Theory of Inverse Problems, Springer-Verlag, New York, 1996.
[14] H.W. Engl, M. Hanke, A. Neubauer, Regularization of Inverse Problems, Kluwer Academic Publishers, Dordrecht, Netherlands, 1996.
[15] Z. Hou, Q. Jin, Tikhonov regularization for nonlinear ill-posed problems, Nonlinear Anal. Theory Methods Appl. 28 (11) (1997) 1799–1809.
[16] S.W. Provencher, A constrained regularization method for inverting data represented by linear algebraic or integral equations, Comput. Phys. Commun. 27 (1982) 213–227.
[17] S.W. Provencher, Contin: a general purpose constrained regularization program for inverting noisy linear algebraic and integral equations, Comput. Phys. Commun. 27 (1982) 229–242.
[18] S.W. Provencher, P. Štěpánek, Global analysis of dynamic light scattering autocorrelation functions, Part. Part. Syst. Char. 5 (1996) 291–294.
[19] G.H. Golub, M. Heath, G. Wahba, Generalized cross-validation as a method for choosing a good ridge parameter, Technometrics 21 (2) (1979) 215–223.
[20] C.G. Farquharson, D.W. Oldenburg, A comparison of automatic techniques for estimating the regularization parameter in non-linear inverse problems, Geophys. J. Int. 156 (2004) 411–425.
[21] P.C. Hansen, D.P. O'Leary, The use of the l-curve in the regularization of discrete ill-posed problems, SIAM J. Sci. Comput. 14 (1993) 1487–1503.
[22] P.C. Hansen, Regularization tools: a Matlab package for analysis and solution of discrete ill-posed problems, Numer. Algorithms 6 (1994) 1–35.
[23] D.E. Koppel, Analysis of macromolecular polydispersity in intensity correlation spectroscopy: the method of cumulants, J. Chem. Phys. 57 (1972) 4814–4820.
[24] V.D.G. Gonzalez, L.M. Gugliotta, J.R. Vega, G.R. Meira, Contamination by larger particles of two almost-uniform latexes: analysis by combined dynamic light scattering and turbidimetry, J. Colloid Interface Sci. 285 (2) (2005) 581–589.
[25] L.M. Gugliotta, G.S. Stegmayer, L.A. Clementi, V.D.G. Gonzalez, R.J. Minari, J.R. Leiza, J.R. Vega, A neural network model for estimating the particle size distribution of dilute latex from multiangle dynamic light scattering measurements, Part. Part. Syst. Char. 26 (2009) 41–52.
[26] J. Kaipio, E. Somersalo, Statistical and Computational Inverse Problems, Springer-Verlag, New York, 2005.
[27] N. Armstrong, D.B. Hibbert, An introduction to Bayesian methods for analyzing chemistry data part I: an introduction to Bayesian theory and methods, Chem. Intell. Lab. Syst. 97 (2009) 194–210.
[28] D.B. Hibbert, N. Armstrong, An introduction to Bayesian methods for analyzing chemistry data part II: a review of applications of Bayesian methods in chemistry, Chem. Intell. Lab. Syst. 97 (2009) 211–220.
[29] C.A.A. Mota, H.R.B. Orlande, M.O.M. Carvalho, V. Kolehmainen, J.P. Kaipio, Bayesian estimation of temperature-dependent thermophysical properties and transient boundary heat flux, Heat Transfer Eng. 31 (7) (2010) 570–580.
[30] D.S. Xue, M.S. Si, Bayesian inference approach to particle size distribution estimation in ferrofluids, IEEE Trans. Magn. 42 (2006) 3657–3660.
[31] G. Lei, K.R. Shao, Y.B. Li, G.Y. Yang, Y. Guo, J. Zhu, J.D. Lavers, Bayesian inversion method and its information determination for the estimation of particle size distribution in ferrofluids, IEEE Trans. Magn. 45 (10) (2009) 3981–3984.
[32] T. Inagaki, E.T. Arakawa, R.N. Hamm, M.W. Williams, Optical properties of polystyrene from the near infrared to the x-ray region and convergence of optical sum rules, Phys. Rev. B 15 (1977) 3243–3253.
[33] M. Kerker, The Scattering of Light and Other Electro-Magnetic Radiation, Academic Press, New York, 1969.
[34] C.F. Bohren, D.H. Huffman, Absorption and Scattering of Light by Small Particles, John Wiley & Sons, New York, 1983.